First measurement of elastic, inelastic and total cross-section at þÿ" s = 1 3 T e V b y T O T E M a n d o v e r v i e w o f c r o s s - s e c LHC energies : TOTEM Collaboration

TOTEM Collaboration

2019-02-01

Eur. Phys. J. C (2019) 79:103
https://doi.org/10.1140/epjc/s10052-019-6567-0

THE EUROPEAN PHYSICAL JOURNAL C

Regular Article - Experimental Physics

First measurement of elastic, inelastic and total cross-section at $\sqrt{s} = 13$ TeV by TOTEM and overview of cross-section data at LHC energies

TOTEM Collaboration

G. Antchev[20], P. Aspell[17], I. Atanassov[20], V. Avati[15,17], J. Baechler[17], C. Baldenegro Barrera[19], V. Berardi[8,9], M. Berretti[4], E. Bossini[14], U. Bottigli[14], M. Bozzo[11,12], H. Burkhardt[17], F. S. Cafagna[8], M. G. Catanesi[8], M. Csanád[6,21], T. Csörgő[6,7], M. Deile[17], F. De Leonardis[8,10], A. D'Orazio[8,10], M. Doubek[3], D. Druzhkin[17], K. Eggert[18], V. Eremin[23], F. Ferro[11], A. Fiergolski[17], F. Garcia[4], V. Georgiev[1], S. Giani[17], L. Grzanka[15,22], J. Hammerbauer[1], J. Heino[4], P. Helander[4,5], T. Isidori[19], V. Ivanchenko[16], M. Janda[3], A. Karev[17], J. Kašpar[2,13], J. Kopal[17], V. Kundrát[2], S. Lami[13], G. Latino[14], R. Lauhakangas[4], R. Linhart[1], C. Lindsey[19], M. V. Lokajíček[2], L. Losurdo[14], M. Lo Vetere[11,12], F. Lucas Rodríguez[17], M. Macrí[11], M. Malawski[15], N. Minafra[19], S. Minutoli[11], T. Naaranoja[4,5], F. Nemes[6,17,a], H. Niewiadomski[18], T. Novák[7], E. Oliveri[17], F. Oljemark[4,5], M. Oriunno[24], K. Österberg[4,5], P. Palazzi[17], V. Passaro[8,10], Z. Peroutka[1], J. Procházka[2], M. Quinto[8,9], E. Radermacher[17], E. Radicioni[8], F. Ravotti[17], E. Robutti[11], C. Royon[19], G. Ruggiero[17], H. Saarikko[4,5], A. Scribano[13], J. Siroky[1], J. Smajek[17], W. Snoeys[17], R. Stefanovitch[17], J. Sziklai[6], C. Taylor[18], E. Tcherniaev[16], N. Turini[14], V. Vacek[3], J. Welti[4,5], J. Williams[19], P. Wyszkowski[15], J. Zich[1], K. Zielinski[15]

[1] University of West Bohemia, Pilsen, Czech Republic
[2] Institute of Physics of the Academy of Sciences of the Czech Republic, Prague, Czech Republic
[3] Czech Technical University, Prague, Czech Republic
[4] Helsinki Institute of Physics, University of Helsinki, Helsinki, Finland
[5] Department of Physics, University of Helsinki, Helsinki, Finland
[6] Wigner Research Centre for Physics, RMKI, Budapest, Hungary
[7] EKU KRC, Gyöngyös, Hungary
[8] INFN Sezione di Bari, Bari, Italy
[9] Dipartimento Interateneo di Fisica di Bari, Bari, Italy
[10] Dipartimento di Ingegneria Elettrica e dell'Informazione-Politecnico di Bari, Bari, Italy
[11] INFN Sezione di Genova, Genoa, Italy
[12] Università degli Studi di Genova, Genoa, Italy
[13] INFN Sezione di Pisa, Pisa, Italy
[14] Università degli Studi di Siena and Gruppo Collegato INFN di Siena, Siena, Italy
[15] AGH University of Science and Technology, Kraków, Poland
[16] Tomsk State University, Tomsk, Russia
[17] CERN, Geneva, Switzerland
[18] Department of Physics, Case Western Reserve University, Cleveland, OH, USA
[19] The University of Kansas, Lawrence, USA
[20] INRNE-BAS, Institute for Nuclear Research and Nuclear Energy, Bulgarian Academy of Sciences, Sofia, Bulgaria
[21] Department of Atomic Physics, ELTE University, Budapest, Hungary
[22] Institute of Nuclear Physics, Polish Academy of Science, Kraków, Poland
[23] Ioffe Physical-Technical Institute of Russian Academy of Sciences, St. Petersburg, Russian Federation
[24] SLAC National Accelerator Laboratory, Stanford, CA, USA

Received: 6 November 2018 / Accepted: 4 January 2019

Abstract The TOTEM collaboration has measured the proton–proton total cross section at $\sqrt{s} = 13$ TeV with a luminosity-independent method. Using dedicated $\beta^* = 90$ m beam optics, the Roman Pots were inserted very close to the beam. The inelastic scattering rate has been measured by the

M. Lo Vetere: Deceased.

[a] e-mail: frigyes.janos.nemes@cern.ch

Published online: 01 February 2019

T1 and T2 telescopes during the same LHC fill. After applying the optical theorem the total proton–proton cross section is $\sigma_{\text{tot}} = (110.6 \pm 3.4)$ mb, well in agreement with the extrapolation from lower energies. This method also allows one to derive the luminosity-independent elastic and inelastic cross sections: $\sigma_{\text{el}} = (31.0 \pm 1.7)$ mb and $\sigma_{\text{inel}} = (79.5 \pm 1.8)$ mb.

1 Introduction

This paper presents the first measurement of the total proton–proton cross section at a center of mass energy $\sqrt{s} = 13$ TeV; the measurement is luminosity independent.

The TOTEM collaboration has already measured the total proton-proton cross section at $\sqrt{s} = 2.76$ TeV, 7 TeV and 8 TeV, and has demonstrated the reliability of the luminosity-independent method by comparing several approaches to determine the total cross sections [10,12,13,18,21,32]. The method requires the simultaneous measurements of the inelastic and elastic rates, as well as the extrapolation of the latter in the invisible region down to vanishing four-momentum transfer squared $t = 0$.

The TOTEM experimental setup consists of two inelastic telescopes T1 and T2 to detect charged particles coming from inelastic pp collisions and the Roman Pot detectors (RP) to detect elastically scattered protons at very small angles. The inelastic telescopes are placed symmetrically on both sides of Interaction Point 5 (IP5): the T1 telescope is based on cathode strip chambers (CSCs) placed at ± 9 m and covers the pseudorapidity range $3.1 \leq |\eta| \leq 4.7$; the T2 telescope is based on gas electron multiplier (GEM) chambers placed at ± 13.5 m and covers the pseudorapidity range $5.3 \leq |\eta| \leq 6.5$. The pseudorapidity coverage of the two telescopes at $\sqrt{s} = 13$ TeV allows the detection of about 92% of the inelastic events, including events with diffractive mass down to 4.6 GeV. As the fraction of events with all final state particles beyond the instrumented region has to be estimated using phenomenological models, the excellent acceptance in TOTEM minimizes the dependence on such models and thus provides small uncertainty on the inelastic rate measurement.

The Roman Pot (RP) units used for the present measurement are located on both sides of the IP at distances of ± 213 m (near) and ± 220 m (far) from IP5. A unit consists of 3 RPs, two approaching the outgoing beam vertically and one horizontally. The horizontal RP overlaps with the two verticals and allows for a precise relative alignment of the detectors within the unit. The 7 m long lever arm between the near and the far RP units has the important advantage that the local track angles in the x and y-projections perpendicular to the beam direction can be reconstructed with a precision of 2 μrad. A complete description of the TOTEM detector is given in [9,11].

Each RP is equipped with a stack of 10 silicon strip detectors designed with the specific objective of reducing the insensitive area at the edge facing the beam to only a few tens of micrometers. The 512 strips with 66 μm pitch of each detector are oriented at an angle of + 45° (five planes) and − 45° (five planes) with respect to the detector edge facing the beam [36].

2 Data taking and analysis

The analysis is performed on two data samples (DS1 and DS2) recorded in 2015 during a special LHC fill with $\beta^* = 90$ m optics. This special optics configuration is described in detail in [10,14,16,31].

The RP detectors were placed as close as 5 times the transverse beam size (σ_{beam}) from the outgoing beams. The collected events have been triggered by the T2 telescope in either arm (inelastic trigger), by the RP detectors in a double-arm coincidence (elastic trigger), and by random bunch crossings (zero-bias sample used for calibration). In DS2 there are no zero-bias data recorded, and the closest run with zero-bias data is used for calibration; the time dependence of the zero-bias trigger rate is taken into account with a scale factor measured on the physics data of DS2 itself and the closest run.

2.1 Elastic analysis

2.1.1 Reconstruction of kinematics

The horizontal and vertical scattering angles of the proton at IP5 (θ_x^*, θ_y^*) are reconstructed in a given arm by inverting the proton transport Eq. [16]

$$\theta_x^* = \frac{1}{\frac{\mathrm{d}L_x}{\mathrm{d}s}} \left(\theta_x - \frac{\mathrm{d}v_x}{\mathrm{d}s} x^* \right), \quad \theta_y^* = \frac{y}{L_y}, \tag{1}$$

where s denotes the distance from the interaction point, y is the vertical coordinate of the proton's trajectory, θ_x is its horizontal angle at the detector, and x^* is the horizontal vertex coordinate reconstructed as

$$x^* = \frac{L_{x,\text{far}} \cdot x_{\text{near}} - L_{x,\text{near}} \cdot x_{\text{far}}}{d}, \tag{2}$$

where $d = (v_{x,\text{near}} \cdot L_{x,\text{far}} - v_{x,\text{far}} \cdot L_{x,\text{near}})$. The scattering angles obtained for the two arms are averaged and the four-momentum transfer squared is calculated

$$t = -p^2 \theta^{*2}, \tag{3}$$

where p is the LHC beam momentum and the scattering angle $\theta^* = \sqrt{\theta_x^{*2} + \theta_y^{*2}}$.

The coefficients L_x, L_y and v_x of Eqs. (1) and (2) are optical functions of the LHC beam determined by the accelerator magnets. The $\beta^* = 90$ m optics is designed with a large vertical effective length $L_y \approx 263$ m at the RPs placed at 220 m from IP5. Since the horizontal effective length L_x is close to zero at the RPs, its derivative $\mathrm{d}L_x/\mathrm{d}s \approx -0.6$ is used instead. The different reconstruction formula in the vertical and horizontal plane in Eq. (1) is also motivated by their different sensitivity to LHC magnet and beam perturbations.

2.1.2 RP alignment and beam optics

After applying the usual TOTEM alignment methods the residual misalignment is about 10 μm in the horizontal coordinate and about 150 μm in the vertical [17,18]. When propagated to the reconstructed scattering angles, this leads to uncertainties of about 3.4 μrad (horizontal angle) and 0.6 μrad (vertical angle). The beam divergence uncertainty has been convoluted with the vertical alignment for the error propagation.

The nominal optics has been updated from LHC magnet and current databases and calibrated using the observed elastic candidates. The uncertainties of the optical functions are estimated with a Monte Carlo program applying the optics calibration procedure on a sophisticated simulation of the LHC beam and its perturbations. The obtained uncertainty is about 1.2 $^0/_{00}$ for $\mathrm{d}L_x/\mathrm{d}s$ and 2.1 $^0/_{00}$ for L_y [16,31].

The statistical uncertainty of the scattering angles, obtained from the data, is 1.9 ± 0.1 μrad vertically (mainly due to the beam divergence) and 4.9 ± 0.1 μrad horizontally (due to the beam divergence and sensor pitch).

2.1.3 Event selection

The analysis is similar to the procedure performed for the measurement of the elastic cross section at several other LHC energies: 2.76 TeV, 7 TeV and 8 TeV [10,12,13,18,21,32]. The measurement of the elastic rate is based on the selection of events with the following topology in the RP detector system: a reconstructed track in the near and far vertical detectors on each side of the IP such that the elastic signature is satisfied in one of the two diagonals: left bottom and right top (Diag. 1) or left top and right bottom (Diag. 2).

Besides, the elastic event selection requires the collinearity of the outgoing protons in the two arms, the suppression of the diffractive events and the equality of the horizontal vertex position x^* reconstructed from the left and right arms.

Figure 1 shows the horizontal collinearity cut imposing momentum conservation in the horizontal plane with 1 $^0/_{00}$ uncertainty. The cuts are applied at the 4σ level, and they are optimized for purity (background contamination in the selected sample less than 0.1%) and for efficiency (uncertainty of true elastic event selection 0.5%). Figure 2 shows the progressive selection of elastic events after each analysis cut.

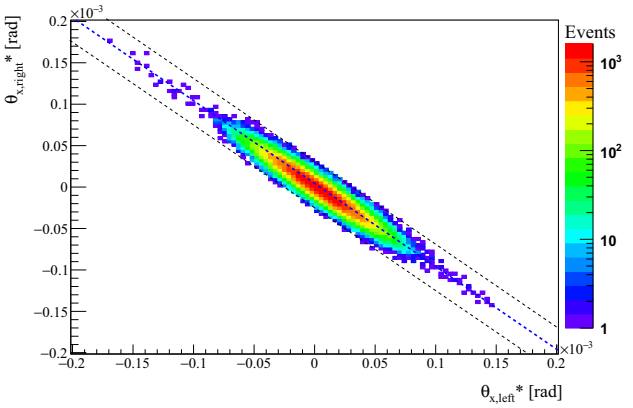

Fig. 1 Analysis cut in the horizontal scattering angle θ_x^*. The blue and black dashed lines represent the mean and the 4σ cuts, respectively

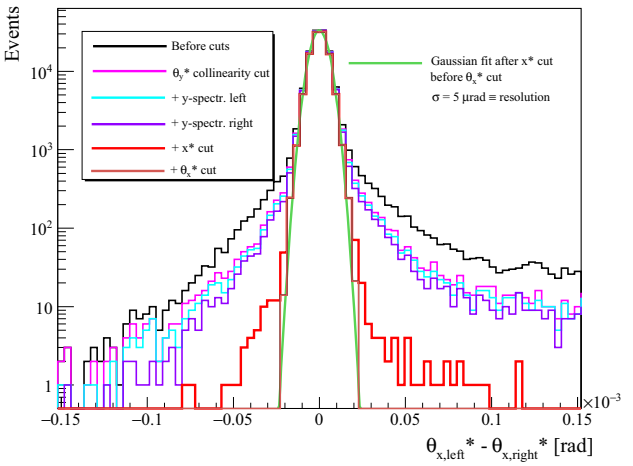

Fig. 2 The distribution of the horizontal scattering angle difference reconstructed from the left and the right arm. The distribution is shown before any analysis cut (black solid line) and after each analysis cut

2.1.4 Geometrical and beam divergence correction, unfolding

The acceptance of elastically scattered protons is limited by the RP silicon detector edge and by the LHC magnet apertures. The proton acceptance correction is calculated taking into account the azimuthal symmetry of elastic scattering, experimentally verified on the data

$$\mathcal{A}(\theta^*) = \frac{2\pi}{\Delta\phi^*(\theta^*)}\,, \tag{4}$$

where $\Delta\phi^*$ is the visible azimuthal angle range, defined by the acceptance cuts. The t-range of the analysis is constrained to $|t|_{\min} = 1.2 \cdot 10^{-2}$ GeV^2 and $|t|_{\max} = 0.2$ GeV^2, a region

Table 1 The t-dependent analysis uncertainties and corrections to the differential elastic rate and to the optical point for both diagonals

	$\|t\|_{\min}$	$\|t\|_{\max}$
Alignment uncertainty	$\pm 1.3\%$	$\pm 3.4\ \%$
Optics uncertainty	$\pm 1^0/_{00}$	$\pm 1^0/_{00}$
$\mathcal{A}(\theta^*)$	$5.96 \pm 3 \times 10^{-2}$	$2.31 \pm 1 \times 10^{-2}$
$\mathcal{D}(\theta_y^*)$	$1.03 \pm 2 \times 10^{-2}$	$1.00 \pm 1 \times 10^{-3}$
$\mathcal{U}(\theta^*)$	$1.002 \pm 5 \times 10^{-5}$	$1.04 \pm 8 \times 10^{-4}$

where the acceptance correction factor $\mathcal{A}(\theta^*)$ is below six in order to limit the systematic error on the final cross section.

Close to the acceptance edges the assumed azimuthal symmetry has to be corrected due to the beam divergence. This additional acceptance loss is modelled with a Gaussian distribution, with experimentally determined parameters, and taken into account as a function of the vertical scattering angle $\mathcal{D}(\theta_y^*)$.

The unfolding of resolution effects is estimated with a Monte Carlo simulation whose parameters are obtained from the data, see Sect. 2.1.2. The angular spread of the beam is determined with an uncertainty 0.1 μrad by comparing the scattering angles reconstructed from the left and right arm, therefore the unfolding correction factor $\mathcal{U}(\theta^*)$ can be calculated with a precision better than 0.1%. The event-by-event correction factor due to acceptance corrections and resolution unfolding is

$$\mathcal{C}(\theta^*, \theta_y^*) = \mathcal{A}(\theta^*)\mathcal{D}(\theta_y^*)\mathcal{U}(\theta^*)\,, \tag{5}$$

see Table 1.

2.1.5 Inefficiency corrections

The proton reconstruction efficiency of the RP detectors is evaluated directly from the data. The strip detectors are not able to resolve multiple tracks, which is the main source of detector inefficiency. The additional tracks can be caused by interactions of the protons with the sensors or the surrounding material or by the pileup with non-signal protons.

The inefficiency corrections are calculated for different categories: "uncorrelated" ($\mathcal{I}_{3/4}$) when one RP out of four along a diagonal has no reconstructed track; this inefficiency includes the loss of the track due to nuclear interaction, shower or pile-up with beam halo and is calculated as a function of θ_y^* per RP [17]. The inefficiency is called "correlated" ($\mathcal{I}_{2/4}$) when both RP of one arm have no reconstructed tracks. The case when two RPs have no reconstructed track in two different arms ($\mathcal{I}_{2/4\,\text{diff.}}$) is derived with a probability formula from the "uncorrelated" inefficiency. The numerical values of these corrections are listed in Table 2.

Table 2 Corrections to the differential and total elastic rate for the different datasets and diagonals. The "uncorrelated" inefficiency correction ($\mathcal{I}_{3/4}$) is θ_y^* dependent, in the table its effect on the elastic rate is provided

Correction [%]	DS1		DS2	
	Diag. 1	Diag. 2	Diag. 1	Diag. 2
$\mathcal{I}_{3/4}$	25.86 ± 0.2	22.04 ± 0.2	20.34 ± 0.1	21.37 ± 0.1
$\mathcal{I}_{2/4}$	19.91 ± 0.2	16.16 ± 0.2	16.09 ± 0.2	17.11 ± 0.2
$\mathcal{I}_{2/4\,\text{diff.}}$	2.38 ± 0.05	1.61 ± 0.04	1.33 ± 0.02	1.5 ± 0.02
η_d	80.93 ± 0.01		99.95 ± 0.01	
η_tr	99.9 ± 0.1		99.9 ± 0.1	

The total correction factor per event is

$$f(\theta^*, \theta_y^*) = \frac{1}{\eta_\text{d}\eta_\text{tr}} \cdot \frac{\mathcal{C}(\theta^*, \theta_y^*)}{1 - \mathcal{I}} \cdot \frac{1}{\Delta t}\,, \tag{6}$$

where the track reconstruction inefficiencies are summed $\mathcal{I} = \mathcal{I}_{3/4}(\theta_y^*) + \mathcal{I}_{2/4} + \mathcal{I}_{2/4\,\text{diff}}$ since they are mutually exclusive, Δt is the bin width and η_d, η_tr are the DAQ and trigger efficiency, respectively. The data sample DS1 had a lower DAQ efficiency compared to DS2 due to the inclusion of the T1 detector in the DAQ that limited the data taking rate. The observed $N_{\text{el,obs}}$ and the fully corrected elastic rate N_el is summarized for the two data sets in Table 4, together with their optical point $\mathrm{d}N_\text{el}/\mathrm{d}t|_{t=0}$.

2.2 Analysis of inelastic scattering

The analysis procedure is similar to the ones for the inelastic event rate measurements at 2.76, 7 and 8 TeV [12,15,21,32] and starts from the number of T2 triggered events as the observed inelastic rate. The events are classified according to their topology: events with tracks in T2 in both hemispheres ("2h"), dominated by non-diffractive minimum bias and double diffraction, and events with tracks in one hemisphere only ("1h"), dominated by single diffraction. Due to the non-operational half-arm of T2 on the negative side, for the 1h category each of the three half-arms are treated separately in the analysis to avoid biases and then the two half-arms on the positive side are combined.

To evaluate the total inelastic rate, several corrections have to be applied. First, to obtain the T2 visible inelastic rate (N_{T2vis}), the observed rate is corrected for beam gas background, trigger, reconstruction efficiency and the effect of pileup. Next, the rate corresponding to the events with at least one final state particle in $|\eta| < 6.5$ ($\text{N}_{|\eta|<6.5}$) is derived by assessing topologies which can cause an undetected event in T2. These are events detected only by T1, central diffractive events with all final state particles outside the T2 acceptance and events with a local rapidity gap covering T2. Finally, to

Table 3 Corrections and systematic uncertainties of the inelastic rate measurement. The second column shows the size of the correction, the third column the systematic uncertainty related to the source

Source	Correction	Uncertainty	Effect on
Beam gas	−0.4%	0.2%	All rates
Trigger efficiency	1.2%	0.6%	All rates
Pile up	3.6%	0.4%	All rates
T2 event reconstruction	0.9 (1.6)%	0.45 (0.8)%	N_{inel}, $N_{\|\eta\|<6.5}$ (N_{T2vis})
T1 only	1.7%	0.4%	N_{inel}, $N_{\|\eta\|<6.5}$
Central diffraction	0.5%	0.35%	N_{inel}, $N_{\|\eta\|<6.5}$
Local rapidity gap covering T2	0%	0.4%	N_{inel}, $N_{\|\eta\|<6.5}$
Low mass diffraction seen	− 0.6%	0.3%	N_{inel}, $N_{\|\eta\|<6.5}$
Low mass diffraction	7.1%	3.55%	N_{inel}

Table 4 The observed elastic $N_{el,obs}$ and inelastic rate $N_{inel,obs}$, the fully corrected elastic N_{el} and inelastic rate N_{inel} and the optical point $dN_{el}/dt|_{t=0}$ of the two data sets (errors where quoted are statistical and systematic)

Data set	Unit	DS1	DS2
$N_{el,obs}$		105729	216825
$N_{inel,obs}$		773000	1488343
N_{el}		$4.273 \cdot 10^5 \pm 0.5\% \pm 2.3\%$	$6.660 \cdot 10^5 \pm 0.5\% \pm 2.3\%$
$dN_{el}/dt\|_{t=0}$	$[GeV^{-2}]$	$8.674 \cdot 10^6 \pm 0.4\% \pm 1.6\%$	$1.356 \cdot 10^7 \pm 0.4\% \pm 1.6\%$
N_{inel}		$1.097 \cdot 10^6 \pm 0.1\% \pm 3.7\%$	$1.708 \cdot 10^6 \pm 0.1\% \pm 3.7\%$

estimate the total inelastic rate (N_{inel}), the contribution of low mass diffraction with only final state particles at $|\eta| > 6.5$ is evaluated. The corrections leading to the total inelastic rate measurement are described below and quantified in Table 3 together with their systematic uncertainties, summing up to 3.7%. The observed $N_{inel,obs}$ and fully corrected inelastic rate N_{inel} is shown in Table 4.

2.2.1 Beam gas background

The beam gas background is estimated from events triggered with T2 on the non-colliding bunches and affects only the 1h category. The intensity difference between the colliding and non-colliding bunches is taken into account. Conservatively, half the size of the correction to the overall inelastic rate is taken as systematic uncertainty.

2.2.2 Trigger efficiency

The trigger efficiency is determined from zero bias triggered events, separately for the different event topologies and integrated over all T2 track multiplicities. The systematic uncertainty is evaluated as the variation required on the 1h trigger efficiency to give compatible fractions for left and right arm (after correcting for the non-operational half arm of T2).

2.2.3 Pileup

The pileup correction factor is determined from the zero bias triggered events. The probability to have a bunch crossing with tracks in T2 is about 0.07 from which the probability of having more than two inelastic collisions with tracks in T2 in the same bunch crossing is derived. The systematic uncertainty is assessed from the variation of the probability, within the same dataset, to have a bunch crossing with tracks in T2 and the uncertainty due to the T2 event reconstruction efficiency.

2.2.4 T2 event reconstruction

The T2 event reconstruction inefficiency is estimated using Monte Carlo (MC) generators (PYTHIA8-4C [25], QGSJET-II-04 [35]) tuned with data to reproduce the measured fraction of 1h events, 0.195 ± 0.010. The systematic uncertainty is taken to be half of the correction. In these runs, they are mostly due to events with tracks only in the non-operational T2 half-arm with some additional events due to only neutral particles within the T2 acceptance. A large fraction of the events missed due to T2 reconstruction inefficiency are recuperated with the T1 detector reducing the correction sizably for N_{inel} and $N_{|\eta|<6.5}$.

2.2.5 T1 only

The T1-only correction takes into account events with no reconstructed particles in T2 but tracks reconstructed in T1. The systematic uncertainty is equal to the precision to which this correction can be calculated from the zero-bias sample.

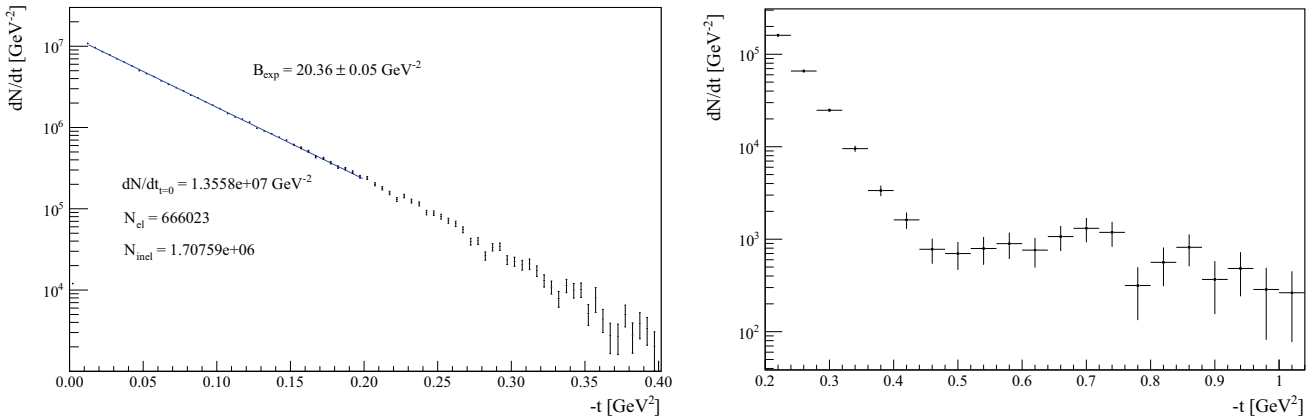

Fig. 3 Differential elastic rate $\mathrm{d}N_{\mathrm{el}}/\mathrm{d}t$ at $\sqrt{s} = 13$ TeV (full physics corrections included) of dataset DS2 with the exponential fit between $|t|_{\min}$ and $|t|_{\max}$. The right panel shows the data in the dip region. The uncertainties shown and quoted are only statistical

2.2.6 Central diffraction

The central diffraction correction, based on the PHOJET and MBR event generators [22,27], takes into account events with all final state particles outside the T1/T2 pseudorapidity acceptance. Both generators are underestimating the low mass resonance contribution. Therefore, the total central diffractive contribution is assumed to be twice the generator estimates. Since the uncertainties of the central diffractive cross-section and the low mass resonance contribution are large, the systematic uncertainty is assumed to be equal to the largest difference of the correction with and without low mass resonance contribution.

2.2.7 Local rapidity gap covering T2

The correction due to local rapidity gap over T2 considers single diffraction events with a rapidity gap of the diffractive system extending over the entire T2 η-range and with no tracks in T1. It is estimated from data, measuring the probability of having a single diffractive-like topology with a gap covering T1 and transferring it to the T2 region correcting for the different conditions (average charged multiplicity, p_T threshold, gap size and surrounding material) between T1 and T2. As a cross-check the correction is also estimated from MC generators (PYTHIA8-4C, QGSJETII-04). The two estimates differ sizably and therefore only a systematic uncertainty equal to the largest estimate is applied, without making any correction.

2.2.8 Low mass diffraction

The T2 acceptance edge at $|\eta| = 6.5$ corresponds to a diffractive mass of about 4.6 GeV (at 50 % efficiency). The low mass diffraction correction, i.e. the contribution of events with all final state particles at $|\eta| > 6.5$, is estimated with QGSJETII-03 [33] after correcting the fraction of 1h events in the MC to the one of the data. At 7 TeV, the estimated correction using this procedure was consistent with the value estimated from data [15]. To account for the large uncertainty of the low mass diffraction contribution and to cover also other predictions [25,29,34], the systematic uncertainty is taken to be half of this correction.

3 Cross sections

3.1 Differential elastic rate and extrapolation to $t = 0$

After unfolding and including all systematic corrections, the physics differential elastic rate $\mathrm{d}N_{\mathrm{el}}/\mathrm{d}t$ is described with an exponential and fitted using the propagated statistical uncertainties in the range between $|t_{\min}|$ and $|t_{\max}|$, see Fig. 3. The normalized χ^2/ndf for the statistical fit is $50.8/36 = 1.4$ as to be expected due to the non-inclusion of the systematic uncertainties. The t-dependent sources of the bin-to-bin correlated systematic uncertainties (described starting from Table 1) are not used in the fit due to their partially non-Gaussian nature and their non-treated interdependencies. This is allowed since their t-dependence is monotonic with the same trend as the statistical errors, thus not changing significantly the relative weight of the bins in the fit and consequently not also the central values for the fitted variables. As a cross-check, the effect of including the systematic uncertainties in the fit has been checked for the extreme points of the range to be sufficient and necessary to bring the χ^2/ndf below 1.

The t-dependent and correlated systematic uncertainties have been propagated from the sources (Table 1), to the measured quantities (Table 4) and the physics results (Table 5) using full MC-based numerical methods, assuring to take in all cases an upper bound in case of unknown interdepen-

Table 5 The nuclear slope B, the cross sections and their systematic and statistical uncertainty. The physics quantities are the weighted average of the DS1 and DS2 measurements

Physics quantity	Value		Total uncertainty
	$\rho = 0.14$	$\rho = 0.1$	
B [GeV^{-2}]	20.36		$5.3 \cdot 10^{-2} \oplus 0.18 = 0.19$
σ_{tot} [mb]	109.5	110.6	3.4
σ_{el} [mb]	30.7	31.0	1.7
σ_{inel} [mb]	78.8	79.5	1.8
$\sigma_{\text{el}}/\sigma_{\text{inel}}$	0.390		0.017
$\sigma_{\text{el}}/\sigma_{\text{tot}}$	0.281		0.009

dencies. As can be noted from the Tables referenced above, such uncertainties are significantly larger, in particular for the slope and the intercept at $t = 0$, than the variation induced by the choice of the fit range, the inclusion of the correlated systematic uncertainties in the χ^2, or due to the deviation of the slope from a pure exponential [17,20]. In fact, even the statistical uncertainties alone are an order of magnitude larger than what is needed to have sensitivity to the expected deviations from the purely exponential.

Assuming that the exponential parameterization holds also for $|t| < |t_{\text{min}}|$ the value of $\mathrm{d}N_{\text{el}}/\mathrm{d}t|_{t=0}$ can be used to determine the total cross-section using Eq. (7).

The magnitude of the systematic effects at $|t| < |t_{\text{min}}|$ for the deviations from the pure exponential functional form and for the Coulomb-nuclear interference, onto the total cross-section, are known from [17–20] and are well contained in the quoted systematic uncertainty in the present paper.

The dip region is shown in the right panel of Fig. 3.

3.2 The total cross section

The measurements of the total inelastic rate N_{inel} and of the total nuclear elastic rate N_{el} (with its extrapolation to $t = 0$, $\mathrm{d}N_{\text{el}}/\mathrm{d}t|_{t=0}$) are combined via the optical theorem to obtain the total cross section in a luminosity independent way

$$\sigma_{\text{tot}} = \frac{16\pi(\hbar c)^2}{1+\rho^2} \cdot \frac{\mathrm{d}N_{\text{el}}/\mathrm{d}t|_{t=0}}{N_{\text{el}} + N_{\text{inel}}}\,, \tag{7}$$

where the parameter ρ is the ratio of the real to the imaginary part of the forward nuclear elastic amplitude.

The total cross section measurements of the DS1 and DS2 data sets have been averaged according to their raw inelastic rate $N_{\text{inel,obs}}$, which yields

$$\sigma_{\text{tot}} = (110.6 \pm 3.4)\ \text{mb}\,, \tag{8}$$

when $\rho = 0.1$ is assumed. The choice of $\rho = 0.1$ in the present analysis is motivated by the results given in [19].

From the measured (and fully corrected) ratio of N_{el} to N_{inel} the luminosity- and ρ-independent ratios

$$\frac{\sigma_{\text{el}}}{\sigma_{\text{inel}}} = 0.390 \pm 0.017, \quad \frac{\sigma_{\text{el}}}{\sigma_{\text{tot}}} = 0.281 \pm 0.009\,, \tag{9}$$

The luminosity independent elastic and inelastic cross sections are derived by combining their ratio and sum

$$\sigma_{\text{el}} = (31.0 \pm 1.7)\ \text{mb}, \quad \sigma_{\text{inel}} = (79.5 \pm 1.8)\ \text{mb}\,. \tag{10}$$

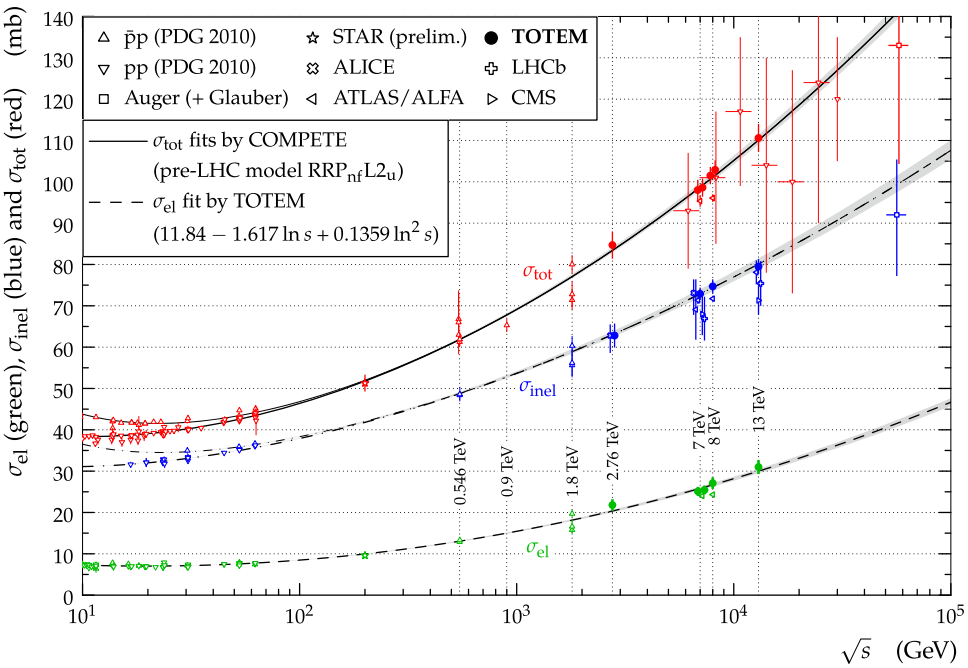

Fig. 4 Overview of elastic (σ_{el}), inelastic (σ_{inel}), total (σ_{tot}) cross section for pp and p$\bar{\text{p}}$ collisions as a function of $\sqrt{s}$, including TOTEM measurements over the whole energy range explored by the LHC [1–5,7,8,12–14,17,18,21,23,24,28,30,32]. Uncertainty band on theoretical models and/or fits are as described in the legend. The continuous black lines (lower for pp, upper for p$\bar{\text{p}}$) represent the best fits of the total cross section data by the COMPETE collaboration [26]. The dashed line results from a fit of the elastic cross section data. The dash-dotted lines refer to the inelastic cross section and are obtained as the difference between the continuous and dashed fits

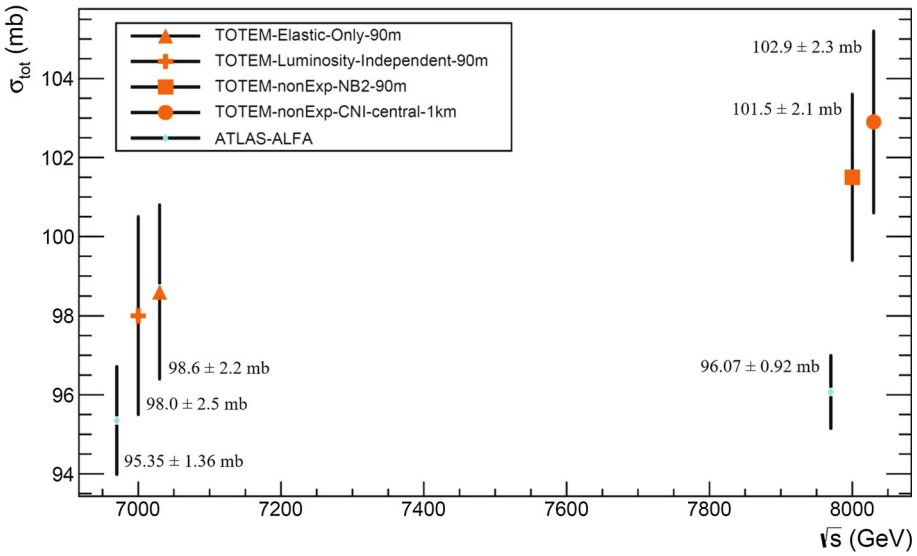

Fig. 5 Focus on the 7–8 TeV range showing the comparison of the pairs of TOTEM measurements which represent the broadest exploration of different methods, data sets, t-range (with or without Coulomb-nuclear interference) and descriptions of the nuclear slope with the ATLAS-ALFA measurements [2,4,13,14,17,18]

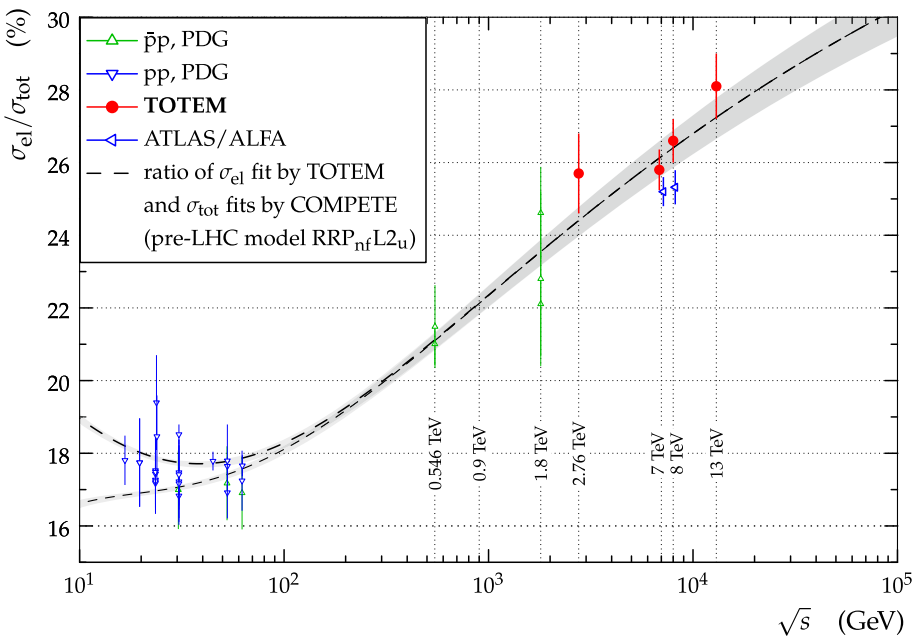

Fig. 6 The elastic to total cross section ratio for pp and p$\bar{\text{p}}$ collisions as a function of $\sqrt{s}$ [2,4,12,13,21,30,32]

The precise inelastic cross-section σ_{inel} measured by TOTEM is compatible with the ATLAS and LHCb results within their uncertainties [1,6].

The measured physics quantities are also calculated for the COMPETE prediction at $\sqrt{s} = 13$ TeV $\rho = 0.14$ [26]. The values obtained for all the physics quantities are summarized in Table 5. Their systematic uncertainties are derived from a full numerical propagation of the individual source of correlated systematic uncertainties shown in Tables 1 and 2.

Figure 4 is the compilation of all the previous pp and p$\bar{\text{p}}$ total, elastic and inelastic measurements, together with a selected set of TOTEM measurements. Figure 5 shows a more detailed plot of the measurements in the range between 7 and 8 TeV including TOTEM values for σ_{tot} obtained with different methods.

With the present measurement TOTEM has covered a range from $\sqrt{s} = 2.76$ to 13 TeV obtaining a variation of total cross-section from (84.7 ± 3.3) to (110.6 ± 3.4) mb and a variation of the nuclear slope B from (17.1 ± 0.3) GeV^{-2} to (20.36 ± 0.19) GeV^{-2} [10,12,13,18,21,32].

The evolution of the elastic to total cross section ratio and the nuclear slope B as function of $\sqrt{s}$ are shown in Figs. 6 and 7. The elastic to total cross section ratio increases with $\sqrt{s}$ as shown by Fig. 6. In particular, the deviation at LHC ener-

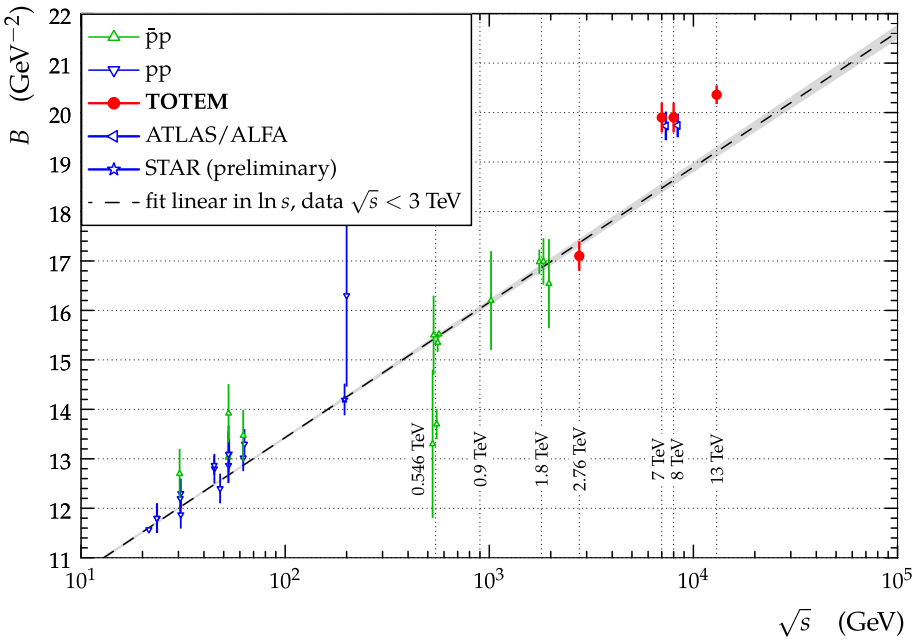

Fig. 7 The nuclear slope B for pp and p$\bar{\text{p}}$ elastic scattering as a function of $\sqrt{s}$. It should be understood that while B is defined at $t = 0$, the experimental measurements are actually averaging the slope, hence they depend on the chosen t-range and on the deviations of the data from a pure exponential. While fluctuations beyond the experimental error bars should thus be expected, the deviation for $\sqrt{s} > 3$ TeV from the linear extrapolation is highly significant [2,4,12,14,21,28,30,32]

gies of the nuclear slope from the low energy linear extrapolation is clearly visible in Fig. 7.

Acknowledgements We are grateful to the beam optics development team for the design and the successful commissioning of the high β^* optics and to the LHC machine coordinators for scheduling the dedicated fills.
This work was supported by the institutions listed on the front page and partially also by NSF (US), the Magnus Ehrnrooth Foundation (Finland), the Waldemar von Frenckell Foundation (Finland), the Academy of Finland, the Finnish Academy of Science and Letters (The Vilho Yrjö and Kalle Väisälä Fund), the OTKA NK 101438 and the EFOP-3.6.1-16-2016-00001 Grants (Hungary). Individuals have received support from Nylands nation vid Helsingfors universitet (Finland), MSMT CR (the Czech Republic), the János Bolyai Research Scholarship of the Hungarian Academy of Sciences and the NKP-17-4 New National Excellence Program of the Hungarian Ministry of Human Capacities.

Data Availability Statement This manuscript has no associated data or the data will not be deposited. [Authors' comment: The data analysed in this manuscript are available from the corresponding author on a reasonable request.]

References

1. M. Aaboud, Measurement of the inelastic proton–proton cross section at $\sqrt{s} = 13$TeV with the ATLAS detector at the LHC. Phys. Rev. Lett. **117**(18), 182002 (2016). https://doi.org/10.1103/PhysRevLett.117.182002. arXiv:1606.02625
2. M. Aaboud, Measurement of the total cross section from elastic scattering in pp collisions at $\sqrt{s} = 8$ TeV with the ATLAS detector. (ATLAS collaboration). Phys. Lett. B **761**, 158–178 (2016b). https://doi.org/10.1016/j.physletb.2016.08.020
3. G. Aad, (ATLAS collaboration). Nat. Commun. **2**, 463 (2011). https://doi.org/10.1016/j.nuclphysb.2014.10.019
4. G. Aad, Measurement of the total cross section from elastic scattering in pp collisions at $\sqrt{s} = 7$ TeV with the ATLAS detector. (ATLAS collaboration). Nucl. Phys. B **889**, 486–548 (2014). https://doi.org/10.1016/j.nuclphysb.2014.10.019
5. R. Aaij et al., Measurement of the inelastic pp cross-section at a centre-of-mass energy of $\sqrt{s} = 7$ TeV. (LHCb collaboration). JHEP **02**, 129 (2015). https://doi.org/10.1007/JHEP02(2015)129
6. R. Aaij et al., Measurement of the inelastic pp cross-section at a centre-of-mass energy of 13 TeV. JHEP **06**, 100 (2018). https://doi.org/10.1007/JHEP06(2018)100. arXiv:1803.10974
7. B. Abelev, Measurement of inelastic, single- and double-diffraction cross sections in proton–proton collisions at the LHC with ALICE. (ALICE collaboration). Eur. Phys. J. C **73**(6), 2456 (2013). https://doi.org/10.1140/epjc/s10052-013-2456-0
8. P. Abreu, Measurement of the proton-air cross-section at $\sqrt{s} =$ 57 TeV with the Pierre Auger Observatory. (Auger collaboration). Phys. Rev. Lett. **109**, 062002 (2012). https://doi.org/10.1103/PhysRevLett.109.062002
9. G. Anelli, The TOTEM experiment at the CERN Large Hadron Collider. (TOTEM collaboration). JINST **3**, S08007 (2008). https://doi.org/10.1088/1748-0221/3/08/S08007
10. G. Antchev et al., First measurement of the total proton-proton cross section at the LHC energy of $\sqrt{s} = 7$ TeV. (TOTEM collaboration). EPL **96**(2), 21002 (2011). https://doi.org/10.1209/0295-5075/96/21002
11. G. Antchev, et al. (TOTEM collaboration), TOTEM Upgrade Proposal (2013). http://cds.cern.ch/record/1554299
12. G. Antchev, et al., Luminosity-Independent Measurement of the Proton-Proton Total Cross Section at $\sqrt{s} = 8$ TeV. (TOTEM collaboration). Phys. Rev. Lett. **111**(1), 012001 (2013). https://doi.org/10.1103/PhysRevLett.111.012001

13. G. Antchev et al., Luminosity-independent measurements of total, elastic and inelastic cross-sections at $\sqrt{s} = 7$ TeV. (TOTEM collaboration). EPL **101**(2), 21004 (2013). https://doi.org/10.1209/0295-5075/101/21004
14. G. Antchev et al., Measurement of proton-proton elastic scattering and total cross-section at $\sqrt{s} = 7$ TeV. (TOTEM collaboration). EPL **101**(2), 21002 (2013). https://doi.org/10.1209/0295-5075/101/21002
15. G. Antchev et al., Measurement of proton-proton inelastic scattering cross-section at $\sqrt{s} = 7$ TeV. (TOTEM collaboration). EPL **101**(2), 21003 (2013). https://doi.org/10.1209/0295-5075/101/21003
16. G. Antchev, LHC optics measurement with proton tracks detected by the Roman Pots of the TOTEM experiment. (TOTEM collaboration). New J. Phys. **16**, 103041 (2014). https://doi.org/10.1088/1367-2630/16/10/103041
17. G. Antchev et al., Evidence for non-exponential elastic proton 2013 proton differential cross-section at low-$|t|$ and $\sqrt{s} = 8$ TeV by TOTEM. (TOTEM collaboration). Nucl. Phys. B **899**, 527–546 (2015). https://doi.org/10.1016/j.nuclphysb.2015.08.010
18. G. Antchev et al., Measurement of elastic pp scattering at $\sqrt{s} = 8$ TeV in the Coulomb-nuclear interference region: determination of the ρ -parameter and the total cross-section. (TOTEM collaboration). Eur. Phys. J. C **76**(12), 661 (2016). https://doi.org/10.1140/epjc/s10052-016-4399-8
19. G. Antchev, et al. First determination of the ρ parameter at $\sqrt{s} = 13$ TeV probing the existence of a colourless three-gluon bound state. (TOTEM collaboration), (CERN-EP-2017-335), (2017) https://cds.cern.ch/record/2298154
20. G. Antchev, et al. Elastic differential cross-section measurement at $\sqrt{s} = 13$ TeV by TOTEM. (TOTEM collaboration), submitted to CERN PH (2018)
21. G. Antchev, et al. Measurement of proton–proton elastic scattering and total cross-section at $\sqrt{s} = 2.76$ TeV. (TOTEM collaboration), in preparation (2018)
22. R. Ciesielski, K. Goulianos, MBR Monte Carlo simulation in PYTHIA8. PoS ICHEP2012:301 (2013)
23. CMS Collaboration (2012) Report No CMS-PAS-FWD-11-001
24. CMS Collaboration (2016) Report No CMS-PAS-FSQ-15-005
25. R. Corke, T. Sjöstrand, Interleaved parton showers and tuning prospects. JHEP **03**, 032 (2011). https://doi.org/10.1007/JHEP03(2011)032
26. J.R. Cudell, V.V. Ezhela, P. Gauron, K. Kang, YuV Kuyanov, S.B. Lugovsky, E. Martynov, B. Nicolescu, E.A. Razuvaev, N.P. Tkachenko, Benchmarks for the forward observables at RHIC, the Tevatron Run II and the LHC. Phys. Rev. Lett. **89**, 201801 (2002). https://doi.org/10.1103/PhysRevLett.89.201801
27. R. Engel, M.A. Braun, C. Pajares, J. Ranft, Diffraction dissociation, an important background to photon–photon collisions via heavy ion beams at LHC. Z. Phys. C **74**, 687–697 (1997). https://doi.org/10.1007/s002880050432
28. W. Guryn, B. Pawlik, Measurement of total and elastic cross sections in p+p collisions at $\sqrt{s} = 200$ gev with the STAR detector at RHIC, (2018) https://indico.cern.ch/event/713101/contributions/3102222/attachments/1704998
29. V.A. Khoze, A.D. Martin, M.G. Ryskin, On minimum-bias effects at the LHC. Phys. Lett. B **679**, 56–59 (2009). https://doi.org/10.1016/j.physletb.2009.07.016
30. K. Nakamura, Review of particle physics. J. Phys. **G37**, 075021 (2010). https://doi.org/10.1088/0954-3899/37/7A/075021
31. F. Nemes, Elastic scattering of protons at the TOTEM experiment at the LHC. PhD thesis, Eötvös U., CERN-THESIS-2015-293 (2015)
32. F. Nemes, Elastic and total cross-section measurements by TOTEM: past and future. PoS (DIS2017) 059 (2017)
33. S. Ostapchenko, QGSJET-II: towards reliable description of very high energy hadronic interactions. Nucl. Phys. Proc. Suppl. **151**, 143–146 (2006). https://doi.org/10.1016/j.nuclphysbps.2005.07.026
34. S. Ostapchenko, Monte Carlo treatment of hadronic interactions in enhanced Pomeron scheme: I. QGSJET-II model. Phys. Rev. D **83**, 014018 (2011). https://doi.org/10.1103/PhysRevD.83.014018. arXiv:1010.1869
35. S. Ostapchenko, QGSJET-II: physics, recent improvements, and results for air showers. EPJ Web Conf. **52**, 02001 (2013). https://doi.org/10.1051/epjconf/20125202001
36. G. Ruggiero, Characteristics of edgeless silicon detectors for the Roman Pots of the TOTEM experiment at the LHC. Nucl. Instrum. Methods A **604**, 242–245 (2009). https://doi.org/10.1016/j.nima.2009.01.056